Topics in Catalysis (2022) 65:1620–1630
https://doi.org/10.1007/s11244-022-01651-0

ORIGINAL PAPER

Role of Polarons in Single-Atom Catalysts: Case Study of Me_1 [Au_1, Pt_1, and Rh_1] on TiO_2(110)

Panukorn Sombut[1] · Lena Puntscher[1] · Marlene Atzmueller[1] · Zdenek Jakub[1] · Michele Reticcioli[2] · Matthias Meier[1,2] · Gareth S. Parkinson[1] · Cesare Franchini[2,3]

Accepted: 31 May 2022 / Published online: 27 June 2022
© The Author(s) 2022

Abstract
The local environment of metal-oxide supported single-atom catalysts plays a decisive role in the surface reactivity and related catalytic properties. The study of such systems is complicated by the presence of point defects on the surface, which are often associated with the localization of excess charge in the form of polarons. This can affect the stability, the electronic configuration, and the local geometry of the adsorbed adatoms. In this work, through the use of density functional theory and surface-sensitive experiments, we study the adsorption of Rh_1, Pt_1, and Au_1 metals on the reduced TiO_2(110) surface, a prototypical polaronic material. A systematic analysis of the adsorption configurations and oxidation states of the adsorbed metals reveals different types of couplings between adsorbates and polarons. As confirmed by scanning tunneling microscopy measurements, the favored Pt_1 and Au_1 adsorption at oxygen vacancy sites is associated with a strong electronic charge transfer from polaronic states to adatom orbitals, which results in a reduction of the adsorbed metal. In contrast, the Rh_1 adatoms interact weakly with the excess charge, which leaves the polarons largely unaffected. Our results show that an accurate understanding of the properties of single-atom catalysts on oxide surfaces requires a careful account of the interplay between adatoms, vacancy sites, and polarons.

Keywords Single-atom catalysis · Density functional theory · Polarons · TiO_2(110) surface · Scanning probe microscope

1 Introduction

Due to their particular local environment, single-atom catalysts (SACs) represent a new frontier in heterogeneous catalysis, resulting in a unique electronic structure in comparison with supported nanoparticle catalysts [1–7]. Metal atoms adsorbed on solid supports and their resulting catalytic properties combine the advantages of homogeneous catalysts (high activity and selectivity) and heterogeneous catalysts (stable and easy to separate), while minimizing the amount of precious metal used in heterogeneous catalysis [3, 8]. Therefore, SACs are expected to bridge the gap between heterogeneous and homogeneous catalysts. However, the tendency of isolated atoms to aggregate into small clusters due to their relatively high surface energy is problematic. A strong covalent metal-support interaction is capable of stabilizing SACs [9]. However, adsorption of SACs in atomic defects on the substrate surface is the most effective way to avoid clustering and stabilize isolated metal atoms on the support [10, 11], expanding the applicability and efficiency of single-atom catalysis.

Nonetheless, such defective surfaces can affect the properties of adsorbed adatoms, whether within or outside the defect itself, and must be carefully investigated. Further, the presence of point defects on transition-metal oxide surfaces can inject excess electrons which can locally couple with ionic vibrations and form small polarons [12]. Adsorbate/oxide-surface interactions are known to be significantly affected by defects and their associated polarons [13–15], but their effect on catalysis has been rarely considered [16, 17]. For instance, the properties of metal atom (Me_1) species on reduced rutile TiO_2(110) surface, a prototypical polaronic system, has been extensively studied as a SAC [18–23], but

✉ Cesare Franchini
cesare.franchini@univie.ac.at

[1] Institute of Applied Physics, TU Wien, 1040 Vienna, Austria

[2] Faculty of Physics, Center for Computational Materials Science, University of Vienna, 1090 Vienna, Austria

[3] Alma Mater Studiorum, Università di Bologna, 40127 Bologna, Italy

the potential effects of polarons are generally neglected. On the reduced TiO_2(110) surface, polarons tend to localize at a 6-fold coordinated Ti atom (Ti_{6c}) in the subsurface layer in the vicinity of the 2-fold coordinated oxygen vacancy (V_{O2c}) site, reducing Ti^{4+} to Ti^{3+} ions [24]. At elevated temperatures, polaron diffusion between subsurface and surface layers may occur, altering the properties and nature of the polaronic state [24–26], and potentially affecting the stability and properties of the adatoms as well.

In recent years, computational studies have become a powerful tool to accurately describe catalytic reactions at the atomic scale in heterogeneous catalysis [27–29]. In particular, first-principles calculations, within the density functional theory (DFT) framework, have revealed several useful insights into the nature of active sites and the reaction mechanisms in the SAC models [30]. Furthermore, the advances brought about by DFT studies facilitate the interpretation of experimental measurements, and might propose specific substrate materials and metal atoms as optimal candidates for efficient SAC processes.

The purpose of this study is to investigate the effect of polarons on the stability and properties of single-metal atom catalysts. We consider the adsorption of Rh_1, Pt_1, and Au_1 transition metals on the reduced rutile TiO_2(110) surface. To investigate the interplay between electron polarons, oxygen vacancies, and the adatom on the TiO_2(110) surface, we performed DFT + U calculations and compared the results with experimental data taken from existing literature (Au_1 [31–35]) as well as new scanning tunneling microscopy data for the Pt_1 and Rh_1 systems. Accordingly, we confirm that charge transfer occurs for Pt_1 and Au_1 adatoms located in O vacancies (V_O), making them the preferred adsorption configurations, by carefully studying the most stable adsorption sites, the appropriate oxidation states, and the interactions among adatoms, O vacancies, and polarons. A low diffusion barrier on the surface of TiO_2(110) allows Pt_1 adatoms to reach O vacancies when dosed in low amount at room temperature. Au_1 adatoms exhibit the same behavior but at a lower temperature with an even lower diffusion barrier. Rh_1 is found to have no preference for such defects, leaving the polarons essentially unaffected in the subsurface. Our results show that the properties of single-atom catalysts on metal-oxide surfaces can be accurately described only by carefully considering the interaction with point defects and polarons, as well as the reduction of the adsorbed metals.

2 Methods

2.1 Computational Methods

All calculations were performed by using the Vienna ab initio simulation package (VASP) [36, 37]. The projector augmented wave method [38, 39] was used for the electron and ion interaction, with the plane-wave basis set cutoff energy set to 400 eV, optimized to include van der Waals interactions as proposed by Dion et al. [40] with the optimized functional (optPBE-DF) [41, 42]. However, DFT calculations have known drawbacks when dealing with electron localization effects [43]. Therefore, it is preferable to use first-principle schemes that account for the localized charge, such as the DFT + U method used here [44, 45]: we dressed the d orbitals of the Ti atoms with an effective on-site Coulomb repulsion term (U_{eff} of 3.9 eV) [46], previously determined by constrained-random-phase-approximation calculations in bulk rutile [25]. The unreconstructed rutile surface was modeled using an asymmetric slab containing five TiO_2 tri-layers in a large two-dimensional 6×2 unit cell and including a vacuum space region greater than 12 Å along the z-axis. The top three tri-layers were allowed to relax, while the bottom two tri-layers were kept fixed at their bulk positions. An alternative slab model in which the broken bonds at the bottom layer were saturated by pseudo-hydrogen atoms did not affect our conclusions regarding the adsorption energies and polaron stabilities. The convergence is achieved when the electronic energy step of 10^{-5} eV is obtained and forces acting on ions become smaller than 0.01 eV/Å. The adsorption energies were computed according to the formula:

$$E_{ads} = E_{TiO_2(110)+adatom} - \left(E_{TiO_2(110)} + E_{adatom}\right)$$

where $E_{TiO_2(110)+adatom}$ is the total energy of the TiO_2(110) surface with the adsorbed adatom, $E_{TiO_2(110)}$ is the total energy of the clean TiO_2(110) surface with an oxygen vacancy and the most stable polaronic configuration [47, 48]. The E_{adatom} represents the energy of the atom in the gas phase. The surface slab is displayed in Fig. 1a.

The diffusion barriers of an adatom on the reduced TiO_2(110) surface were evaluated using the climbing image nudged elastic band (CI-NEB) method [49, 50] with three interpolated images. As initial and end states we carefully selected solutions including adatoms in the same oxidation state.

In order to inspect the different charge states of the metal atoms on different adsorption sites and the effect of the presence of polarons, we adopted the following strategy (see Fig. 2).

(1) To inhibit polaron formation, we manually removed the two excess electrons (changed the flag NELECT in VASP), resulting in a positively charged slab. By doing so, we remove polaron-related energy contributions, such as polaron formation energies or polaron-

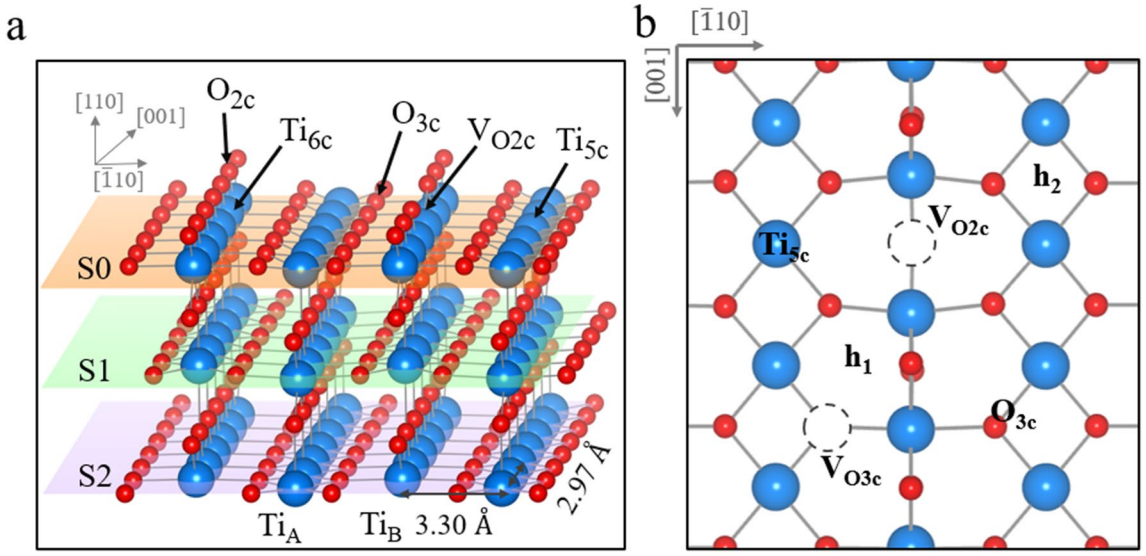

Fig. 1 Structure of the TiO_2(110) surface, Ti atom, O atom, and oxygen vacancy are depicted in big blue sphere, small red sphere and dashed-circle, respectively. **a** Side view of a 6×2 unit cell and **b** top view with possible adsorption sites: a 2-fold oxygen vacancy (V_{O2c}), hollow$_1$ (h_1), hollow$_2$ (h_2), a 5-fold titanium atom (Ti_{5c}), a 3-fold oxygen atom (O_{3c}) and a 3-fold oxygen vacancy (V_{O3c})

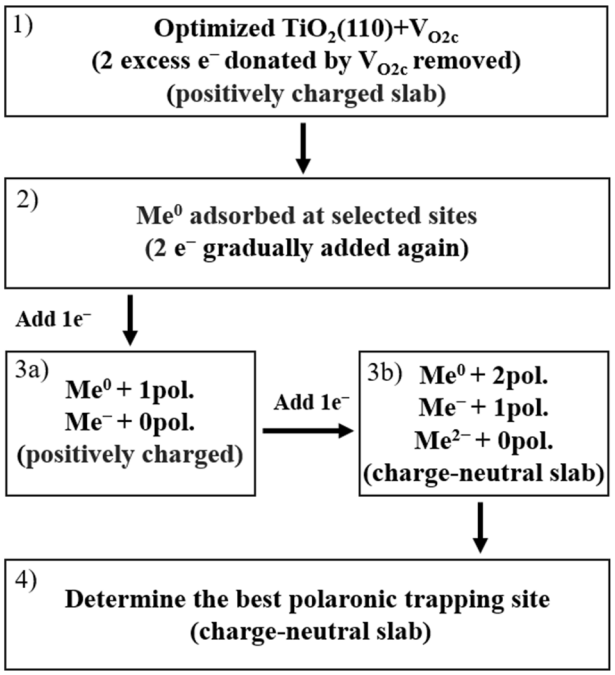

Fig. 2 A flow diagram shows the strategy to obtain the proper charge states of metal atoms adsorbed on different adsorption sites on a charge-neutral reduced TiO_2(110) surface with one V_{O2c}

Me interactions, which allows for a more systematic and controlled approach to study Me single-atom sites.

(2) Adsorption sites were selected based on existing literature [22, 23, 31, 33–35, 51–54] (see Fig. 1). The Me-single atoms are adsorbed at the different adsorption sites as neutral species Me^0 on the previously prepared surface (i.e., without polarons to interact with). The obtained Me^0 adsorption energies can be considered initial reference values.

(3) To account for the variation in relative adsorption strengths due to the oxidation state of the Me_1 atom, charge is slowly re-added to the system. By adding one and then two electrons, the single atom is able to achieve its most favorable oxidation state Me^0, Me^- or Me^{2-}:

(a) Adding one electron: The Me_1 can either retain its additional charge displaying the Me^- oxidation state or become neutral again by moving the electron to the support where it forms a polaron [Me^0 + 1pol.] vs. [Me^- + 0pol.].

(b) Adding two electrons: Me^0, Me^- and Me^{2-} become available oxidation states as a result of adding one more electron. Three different configurations can be obtained: [Me^0 + 2pol.] vs. [Me^- + 1pol.] vs. [Me^{2-} + 0pol.].

As a result of step 3(b), we have retrieved the initial charge neutrality, artificially altered in step 1. At this step, we have ensured that polarons are located at the lowest energy polaronic sites (in S1 in the vicinity of V_{O2c}) as they would in the pristine slab. Therefore, the remaining optimizations left are the interactions of polarons, if present, with the Me single atom, which is covered in step 4. Clearly, if the Me^{2-} state results as the preferred one, no polarons are formed in the slab.

(4) When polarons are formed (Me^0 and Me^-), we inspect the energy stability with respect to different polaronic trapping sites (in S0 and S1). In this way we consider the effect of the spatial polaron-V_{O2c} and polaron-Me separation. It is known that the adatom adsorption energy is affected by the polaron orbital topology, degree of localization, and associated local structural distortions [24]. By comparing the final total energies of these charge-neutral slabs we determine the final ground state structure with the most favorable Me oxidation state previously determined and preferable polaron configurations.

The actual Me oxidation state is determined by counting the number of Ti^{3+} in the charge-neutral slab (i.e. the number of polarons in the slab), the local spin moment at the Me single atom itself, and integrated pDOS.

To selectively control the charge localization in different Ti^{3+} sites, we used the occupation matrix control tool [55], which consists of an initial constrained calculation (with an input occupation matrix kept fixed during the calculation) followed by an unconstrained calculation.

2.2 Experimental Details

Low temperature scanning tunneling microscopy (STM) was performed in a two-vessel UHV chamber consisting of a preparation chamber ($p < 1 \times 10^{-10}$ mbar) and an analysis chamber ($p < 2 \times 10^{-11}$ mbar). The preparation chamber is equipped with a commercial X-ray photoelectron spectroscopy (XPS). The analysis chamber is equipped with an Omicron LT-STM with a Qplus sensor and an in-vacuum preamplifier [56]. Room-temperature STM was performed in a second two-vessel UHV chamber consisting of a preparation chamber ($p < 1 \times 10^{-10}$ mbar) and an analysis chamber ($p < 5 \times 10^{-11}$ mbar). The analysis chamber is equipped with a nonmonochromatic Al Kα X-ray source (VG), a SPECS Phoibos 100 analyzer for XPS, and an Omicron μ-STM. STM in both UHV chambers was conducted in constant current mode with an electrochemically etched W tip on synthetic TiO_2(110) single crystals (from CrysTec GmbH) prepared in UHV by sputtering (1 kV, Ar+, 15 min) and annealing (20 min, 700 °C). Rh and Pt were deposited using an e-beam evaporator (FOCUS), with the flux calibrated using a temperature-stabilized quartz microbalance (QCM). The STM images were corrected of distortion and creep of the piezo scanner as described in ref [57].

3 Results

The rutile TiO_2(110) surface is one of the most intensively studied metal-oxide surfaces [58–60]. This surface layer consists of bridging oxygen rows (O_{2C}) and 5-fold coordinated titanium (Ti_{5c}) rows (see the structural model in Fig. 1). Bridging oxygen vacancies (V_{O2c}) can be easily created in UHV conditions by sputtering and annealing. Each V_{O2c} defect donates two excess electrons to the surface, which are trapped in Ti sites forming small polarons, clearly identified by sharp in-gap peaks [12, 48, 61–63]. We aim to elucidate the impact of polarons on the stability and properties of single-metal atoms (Pt_1, Au_1, and Rh_1) adsorbed on the rutile TiO_2(110) surface. The adsorption sites are labeled in Fig. 1b.

3.1 Pt_1 on the TiO_2(110) Surface

In order to investigate the adsorption of Pt_1 on TiO_2(110), we considered possible adsorption sites as reported in the available literature [21, 22, 51, 52] but including the presence of polarons. Figure 3a-c shows the three most stable adsorption sites and their corresponding calculated projected DOS (pDOS) as well as their oxidation states, taking polaronic effects into account. Pt_1 adsorbed at a bridging oxygen vacancy is the most stable adsorption site ($E_{ads} = -3.22$ eV). The Pt_1 atom in this configuration shows an oxidation state of Pt^{2-} due to the charge transfer of two excess electrons from the reduced surface to the Pt_1 adatom, meaning that it is more favorable to transfer the electrons to Pt_1 rather than using the excess charge to form polarons. The calculated pDOS indeed shows no in-gap Ti polaronic peaks. We note that Pt^- in this configuration is less stable than Pt^{2-} by 0.39 eV (Fig. S6). Pt_1 at the h_1 site is next in energy ($E_{ads} = -2.84$ eV), with Pt^0 being the most stable oxidation state. In this case, the two excess electrons prefer to be trapped in polaronic sites, and no evident net charge transfer to Pt_1 occurs. The pDOS also shows two polaronic in-gap peaks for two Ti^{3+} sites, similar to the clean surface (Fig. S1). When polaron formation is maintained, as in the case of Pt^0, polarons prefer to be trapped near the oxygen vacancy in the S1 layer [24]. The last possible adsorption site with comparatively large adsorption energy is Pt_1 adsorbed atop a 3-fold coordinated oxygen atom on the basal plane. Pt^- is the most stable oxidation state at this site, with one polaron again preferably located in the S1 layer near the oxygen vacancy. Overall, the polarons prefer to be located in the S1 layer in the proximity of the V_{O2c} and maximize their distance with the adsorbed Pt_1 adatom due to the repulsive interaction between the negatively charged polaron and the adsorbed metal atom. A variation of the order of 300 meV

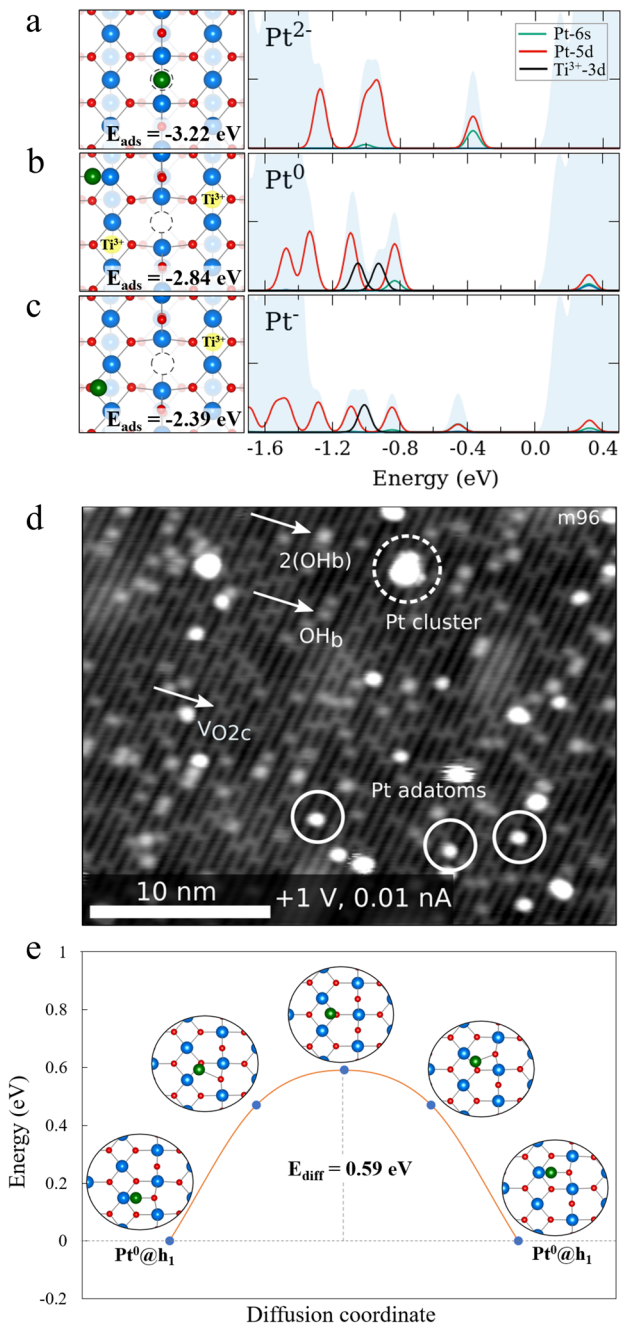

Fig. 3 Minimum energy configuration of possible adsorption sites of Pt_1 on the $TiO_2(110)$ surface. **a** $Pt_1@V_{O2c}$ without polarons resulting in a Pt^{2-} configuration. **b** Pt_1 in h_1 with two polarons resulting in a Pt^0 configuration. **c** Pt_1 atop O_{3C} atom with one polaron resulting in a Pt^- configuration, where O, Ti^{4+}, Ti^{3+}(polaron), Pt_1 are small red, big blue, big yellow, big green spheres and V_O is a dashed-circle, respectively. Each configuration is aligned with its respective DOS panels, where the total DOS, pDOS of Pt (5d), pDOS of Pt (6s), and pDOS of Ti^{3+}(3d, polarons) are filled light blue, red line, green line, and black line, respectively. **d** Empty-state room temperature STM images of 0.007 ML Pt on the reduced rutile $TiO_2(110)$ surface deposited at room temperature, with surface oxygen vacancies (V_{O2c}), OH groups (OH_b), pairs of OH groups ($2(OH_b)$), Pt adatoms (circle) and Pt clusters (dashed circle) labelled in the image. **e** Diffusion path of Pt_1 adatom on $TiO_2(110)$ from one hollow site to the next in the neighboring unit cell without the perturbation from any V_O

in the adatom adsorption energy can be seen depending on polaron position and its distance to the adatom (Fig. S2).

The room-temperature STM image (Fig. 3d) shows Pt_1 adsorbed on the reduced rutile $TiO_2(110)$ surface. The $TiO_2(110)$ surface is characterized in STM by bright rows of 5-fold coordinated Ti^{4+} alternating with dark rows of 2-fold bridging O^{2-}, which run along the [001] direction [60]. Small protrusions over the dark rows can be assigned to oxygen vacancies V_{O2c}, and brighter features on the dark rows can be assigned to bridging OH [64] and pairs of bridging OH. These originate from water dissociation at the V_{O2c} [65–67]. Pt adatoms can be stabilized at low coverage, but clusters dominate the higher the coverage. The Pt adatoms adsorb in the 2-fold oxygen vacancies (marked in circle), which can be identified directly when rare events of adatoms diffusion occur. In this case, the Pt adatom diffuses from one V_O to another (Fig. S7). Both the initial and final vacancies are imaged in STM. Dosing water or oxygen gas (O_2) at room temperature (2 L; 100 s 2×10^{-8} mbar) prior to the Pt deposition leads to the reparation of the V_O site [66–68]. In such an experiment, only Pt clusters are observed (as seen in Fig. S8). These results show the direct correlation between oxygen vacancies and the Pt adatoms stabilization.

In order to account for dynamical effects involving diffusion of the metal species, we calculated the diffusion barrier of the adsorbed Pt_1 along the [001] direction. The calculated energy barrier is low (0.59 eV, see Fig. 3e) so that Pt_1 can diffuse already at room temperature and reach the best adsorption site (at the oxygen vacancies). The calculated results are therefore in-line with our room-temperature STM images, where only Pt_1 at oxygen vacancies have been observed on the reduced $TiO_2(110)$ surface at low coverage. At lower dosing temperature, possible metastable adsorption configurations outside the V_{O2c} can exist.

3.2 Au_1 on the $TiO_2(110)$ Surface

Au_1 adsorbed on $TiO_2(110)$ exhibits a similar structure than Pt_1, as shown in Fig. 4. The most stable adsorption site for Au_1 is located at V_{O2c} ($E_{ads} = -2.06$ eV). Au_1 located at this site becomes negatively charged with an oxidation state of Au^-. Polaronic configurations are most favorable when the remaining polaron forms in the S1 layer close to the V_{O2c} (Fig. 4a). We also considered the on-top 5-fold Ti atom adsorption site, as it was previously considered in other theoretical works [31, 32, 69]. The most stable valence state of Au_1 at this site is Au^- with one polaron remaining in the S1 layer close to $V_{O2c,}$ as shown in Fig. 4b ($E_{ads} = -1.46$ eV). The calculated pDOS in both cases shows that the valence d and s states are filled, with one characteristic in-gap polaronic peak. Similarly to Pt_1, the different polaronic configurations can modify the adsorption energy up to 300 meV (Figs. S3, S4).

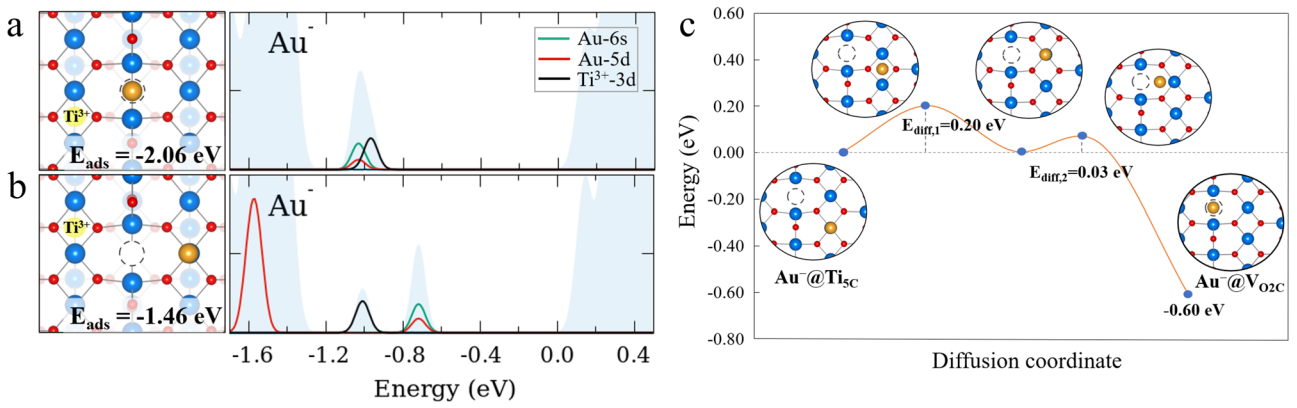

Fig. 4 Minimum energy configuration of possible adsorption sites of Au_1 on the $TiO_2(110)$ surface. **a** $Au_1@V_{O2c}$ with one polaron resulting in a Au^- configuration. **b** Au_1 atop Ti_{5c} atom with one polaron resulting in a Au^- configuration. Each configuration is aligned with its respective DOS panels, where the total DOS, pDOS of Au (5d), pDOS of Au (6s), and pDOS of Ti^{3+}(3d, polarons) are filled light blue, red line, green line, and black line, respectively. **c** Diffusion path of Au_1 atom on $TiO_2(110)$ from atop Ti_{5c} to the V_{O2c} site, where O, Ti^{4+}, Ti^{3+}(polaron) and Au_1 are small red, big blue, big yellow and big yellow-brown spheres, and V_O is a dashed-circle, respectively

The diffusion barrier of Au_1 on the $TiO_2(110)$ from the 5-fold Ti atom to the next 5-fold Ti atom along [001] direction is low (0.2 eV), and even lower is the corresponding barrier for diffusing from the 5-fold Ti atom to the oxygen vacancy which is almost barrierless, indicating a facile diffusion (Fig. 4c). Based on our results, we can conclude that at very low Au coverage, all Au_1 adatoms will be trapped in the oxygen vacancies on the surface. This result agrees with the room temperature STM measurement at low coverage [35] and with the observation of the nucleation of gold clusters at oxygen vacancy sites at high coverage [31, 32].

3.3 Rh_1 on the $TiO_2(110)$ Surface

We studied the adsorption of Rh_1 adatoms on $TiO_2(110)$ by combining DFT + U calculations with XPS and STM experiments. The adsorption sites with their respective adsorption energy are summarized in Fig. 5. Interestingly, Rh_1 adsorbed at V_{O2c} (Fig. 5c) is not the preferential configuration ($E_{ads} = -2.82$ eV). We assign a Rh^- state to this configuration, due to the presence of an in-gap polaronic peak from one Ti^{3+} atom. Two configurations at hollow sites are shown in Fig. 5a and b. The oxidation state of the Rh_1 adatom at hollow sites depends on the nearest oxygen atoms binding to it. For instance, the relaxed structures show that Rh^0 binds to the O_{3c} and O_{2c} atoms ($E_{ads} = -3.24$ eV), whereas the Rh^- at the hollow site near V_{O2c} binds to only the O_{3c} atom ($E_{ads} = -3.05$ eV). A charge transfer occurs for Rh_1 near the V_{O2c} where one excess electron transfers to Rh_1, leaving the second excess electron to form a polaron in the S1 layer near V_{O2c}. The pDOS also shows that there is one characteristic in-gap polaronic peak. The Rh_1 at a hollow site that is distant from V_{O2c} is assigned to Rh^0 and has two remaining polarons in a preferential S1 configuration. The calculated pDOS shows the two in-gap polaronic peaks from Ti^{3+} atoms. Polarons reside in the S1 layer minimizing the distance from V_{O2c} while maximizing the distance from the Rh_1. However, the adsorption energies of Rh^0 and Rh^- are almost degenerate.

The adsorption of an adatom at the 3-fold oxygen vacancy (V_{O3c}) has been proposed to rationalize the result from scanning transmission electron microscopy (STEM) experiments and DFT calculations for Pt_1 and Rh_1 [22, 23]. Other works argued that this adsorption does not exist on $TiO_2(110)$ due to the energetically unfavorable formation of the 3-fold oxygen vacancy (V_{O3c}) on the bare $TiO_2(110)$ surface [35, 52]. Our calculations also show that the formation of V_{O2c} defects is much more favorable than the V_{O3c} vacancy by 1.39 eV on the pristine surface. Figure S5 shows, however, that when Rh_1 is present and adsorbs at a V_{O3c}, it becomes the most thermodynamically stable adsorption site ($E_{ads} = -3.42$ eV) with respect to the V_{2Oc} formation.

Despite the unfavorable 3-fold oxygen vacancy formation energy found for the pristine surface, the presence of adatoms can alter the energetic cost of creating different vacancies other than V_{O2c} and therefore should not be excluded. While Rh_1 in V_{O3c} is the most stable configuration found, the question arises whether it can be reached or not, as the as-prepared surface does not exhibit such defects prior to the deposition of Rh. We calculated the oxygen migration from V_{O2c} to V_{O3c} with the presence of Rh_1 (Fig. 6), ignoring the presence of polarons and changes in the oxidation state of Rh. A barrier of 0.62 eV is obtained, significantly higher than the diffusion of Rh (0.28 eV, Fig. 5d) on the bare surface, suggesting that prior to the formation of in V_{O3c} adsorbed Rh, the adatoms would sinter into clusters (assuming these would be favorable in energy).

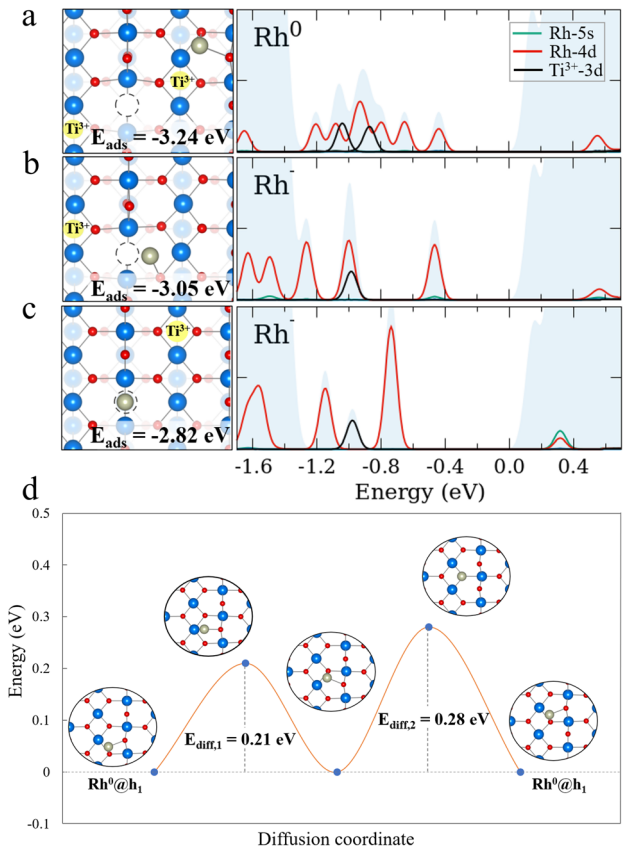

Fig. 5 Minimum energy configuration of possible adsorption sites of Rh_1 on the TiO_2(110) surface. **a** Rh_1 in h_1 with two polarons resulting in a Rh^0 configuration. **b** Rh_1 in h_1 near the V_{O2c} with one polaron resulting in a Rh^- configuration. **c** $Rh_1@V_{O2c}$ with one polaron resulting in a Rh^- configuration. Each configuration is aligned with its respective DOS panels, where the total DOS, pDOS of Rh (4d), pDOS of Rh (5s), and pDOS of Ti^{3+}(3d, polarons) are filled light blue, red line, green line, and black line, respectively. **d** Diffusion path of Rh_1 atom on TiO_2(110) from the h_1 site to the next h_1 site, where O, Ti^{4+}, Ti^{3+} and Rh_1 are small red, big blue, big yellow and big silver spheres, and V_O is a dashed-circle, respectively

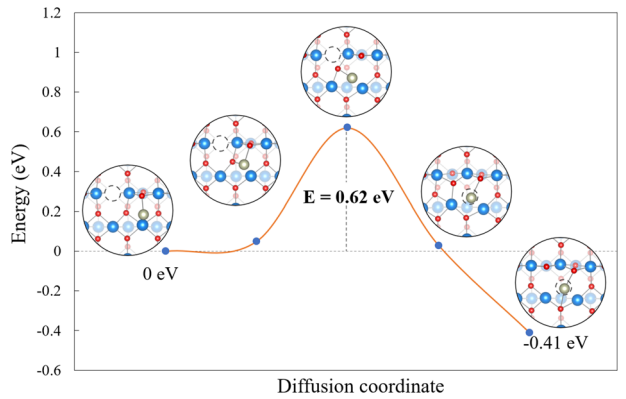

Fig. 6 Energy profile of V_O migration between the initial state (Rh^- at hollow site) and the final state (Rh^- at 3-fold V_O). In order to match the oxidation state of the final state in the NEB, the initial state is set to −1 instead of 0, giving an offset of ~0.2 eV

Figure 7a–c shows STM images of TiO_2(110) before (a) and after deposition of 0.04 ML of Rh (b) and (c) at 100 K, where 1 ML corresponds to 1 Rh atom per surface unit cell. The images were acquired using liquid nitrogen as the cryogen for the LT-STM, giving the sample a temperature of 78 K. Features on the bright Ti^{4+} rows (Fig. 7a, b) with an apparent height of 90–100 pm can be assigned to molecular water adsorbed to Ti^{4+} [70]. Rh adatoms (marked in circles) are located atop the bright Ti^{4+} rows but slightly tilted towards the dark rows (bridging O^{2-}). All Rh adatoms adsorb at the same site but vary in apparent height between 140 and 180 pm. This behavior differs from the behavior of Au and Pt adatoms, which preferentially adsorb in the V_{O2c} of the TiO_2(110) surface [35]. Our data suggest no preferential interaction between Rh and V_{O2c} as the density of the visible V_{O2c} is identical before and after Rh deposition. This result agrees with our DFT calculations, where the best adsorption of Rh_1 is located at the hollow between the bridging oxygen row and the Ti row.

Figure 7d shows XPS spectra and the corresponding STM images of the Rh 3d peak of the as-deposited Rh at 100 K and after subsequent annealing to 873 K. Between 100 K and 150 K the Rh 3d peak shifts to higher binding energy. This core-level shift could be related to a final state effect linked to the small size of the clusters, which appear in STM at 150 K. A similar effect can be recognised when comparing Au_1 and Au_3 to Au nanoparticles on the reduced TiO_2(110) surface. The Au 4f binding energies of the Au_1 and Au_3 are similar to those at a higher coverage of Au. This effect occurs from a cancellation of initial and final state effects for Au_1 and Au_3. By increasing the coverage, the binding energy first decreases and finally increases [71]. Between 150 and 250 K the peak stays the same but when heating the sample to temperatures above 300 K the peak shifts gradually to lower binding energy. This is related to the formation of bigger clusters with increasing temperature. These experimental observations, where Rh is seen to cluster after heating just to 150 K (Fig. 7d) agree with our previous calculated diffusion barriers and preference to sintering.

4 Discussion and Conclusions

The presence of localized charges on surfaces in form of small polarons, unavoidably impacts adsorption and reaction processes and surface dynamics. Previous studies have shown that adsorbed CO exhibit different coupling regime (from attractive to repulsive) depending on the position and density of small polarons, revealing a polaron-mediated correlation between CO adsorption energy and reduction state of the sample [13]. Substantial polaron-charge transfer has been found in O_2 adsorption, leading to the formation

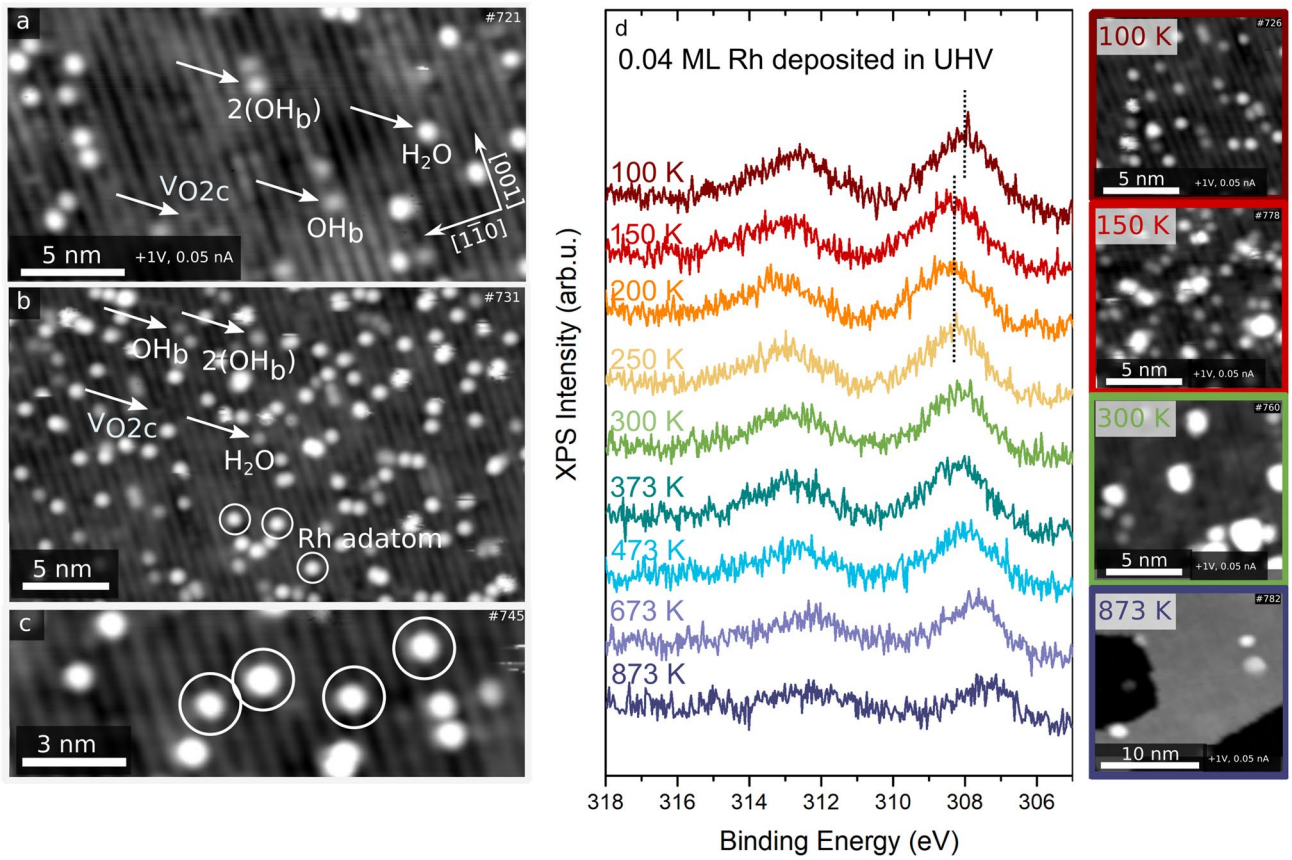

Fig. 7 Experimental investigation of 0.04 ML Rh adsorbed on TiO_2(110). **a** STM image (acquired at 78 K) of the clean TiO_2(110) surface. Surface oxygen vacancies (V_{O2c}), OH groups (OH_b), pairs of OH groups ($2(OH_b)$), and adsorbed water (H_2O) molecules can be seen. **b** and **c** Following the evaporation of 0.04 ML Rh at 100 K, Rh adatoms (circle) can be seen. **d** XPS spectra and STM images of the Rh 3d peak after gradually increasing the temperature

of superoxo and peroxo species [14]. Here, we have shown that single-atom adsorption is also strongly coupled with polaron-charge transfer effect, which affects the adsorption energy and, importantly, the oxidation state of the metal atoms. For example, a Pt^{2-} binds stronger than a Pt^{-} at the V_O site by 0.39 eV. This also implies that the reduction level and associated polaron density does affect the stability of the adsorbed metal atoms, and therefore its surface dynamics, but also its reactivity (i.e. charge transfer between the single-atom catalysts and adsorbed molecules).

For our model system, we found that Pt_1 and Au_1 adatoms have low diffusion barriers and preferably adsorb in V_{O2c}. At higher dosing amounts, clusters can be observed. Rather than forming polarons, the V_{O2c} excess electrons are transferred to the metal atoms, altering their electronic structure by filling their valence states and result in modifying their relative stabilities. The fact that negatively Pt_1 and Au_1 adatoms form cluster means that during the diffusion process there must be a substantial charge transfer from the Pt_1 and Au_1 adatoms to the substrate [72, 73]. Rh_1 adatoms, however show no preference for the V_{O2c} defect, leaving the excess charge to form polarons and instead adsorb at hollow sites, which is in agreement with our experimental STM observations where they quickly sinter into clusters with increasing temperature at low coverage.

The interaction between adsorbates and polarons is further complicated by the presence of additional species which could alter the surface charge balance. In this respect, it is also important to note that the TiO_2(110) surface is fully oxidized under realistic conditions. Therefore, V_O is repaired by H_2O or O_2 molecules, leading to hydroxylated TiO_2(110) or oxidized TiO_2(110) surfaces. The oxidized TiO_2(110) surface was suggested to bind Au_1 stronger than the V_O site on the reduced TiO_2(110) surface [53]. Contrary to the Au case, only Pt clusters were observed on the oxidized TiO_2(110) surface.

Nevertheless, the presence of small polarons is important even for a realistic TiO_2(110) surface, because repair of an oxygen vacancy by H_2O results in two electron polarons arising from two surface OH groups. Clearly, the modeling of such complicated multi-polaron

configurational space (which might also involve the simultaneous formation of electron and hole polarons) is clearly unfeasible via conventional DFT. In order to efficiently explore the energy landscape, novel automated machine-learning based methods must be implemented and employed to determine the most favorable (structural and electronic) configurations and the most likely dynamical paths [74].

Supplementary Information The online version contains supplementary material available at https://doi.org/10.1007/s11244-022-01651-0.

Acknowledgements G.S.P., P.S., L.H., M.M. and M.A. acknowledge funding the European Research Council (ERC) under the European Union's Horizon 2020 research and innovation programme (Grant Agreement No. 864628). Z.J. was supported by the Austrian Science Fund (FWF, Y847-N20, START Prize). C.F., G.S.P., M.R. and M.M. were supported by the Austrian Science Fund (FWF) project SFB TACO (F81). The computational results presented have been achieved by using the Vienna Scientific Cluster.

Funding Open access funding provided by Austrian Science Fund (FWF).

Open Access This article is licensed under a Creative Commons Attribution 4.0 International License, which permits use, sharing, adaptation, distribution and reproduction in any medium or format, as long as you give appropriate credit to the original author(s) and the source, provide a link to the Creative Commons licence, and indicate if changes were made. The images or other third party material in this article are included in the article's Creative Commons licence, unless indicated otherwise in a credit line to the material. If material is not included in the article's Creative Commons licence and your intended use is not permitted by statutory regulation or exceeds the permitted use, you will need to obtain permission directly from the copyright holder. To view a copy of this licence, visit http://creativecommons.org/licenses/by/4.0/.

References

1. Yang X, Wang A, Qiao B, Li JUN (2013) Single-atom catalysts: a new frontier. Acc Chem Res 46:1740–1748
2. Liu J (2017) Catalysis by supported single metal atoms. ACS Catal 7:34–59. https://doi.org/10.1021/acscatal.6b01534
3. Zhang H, Liu G, Shi L, Ye J (2018) Single-atom catalysts: emerging multifunctional materials in heterogeneous catalysis. Adv Energy Mater 8:1–24. https://doi.org/10.1002/aenm.201701343
4. Qiao B, Wang A, Yang X et al (2011) Single-atom catalysis of CO oxidation using Pt1/FeOx. Nat Chem 3:634–641. https://doi.org/10.1038/nchem.1095
5. Jones J, Xiong H, DeLaRiva AT et al (2016) Thermally stable single-atom platinum-on-ceria catalysts via atom trapping. Science 353:150–154. https://doi.org/10.1126/science.aaf8800
6. Liang S, Hao C, Shi Y (2015) The power of single-atom catalysis. ChemCatChem 7:2559–2567. https://doi.org/10.1002/cctc.201500363
7. Gates BC, Flytzani-Stephanopoulos M, DIxon DA, Katz A (2017) Atomically dispersed supported metal catalysts: Perspectives and suggestions for future research. Catal Sci Technol 7:4259–4275. https://doi.org/10.1039/c7cy00881c
8. Chen F, Jiang X, Zhang L et al (2018) Single-atom catalysis: bridging the homo- and heterogeneous catalysis. Cuihua Xuebao Chin J Catal 39:893–898. https://doi.org/10.1016/S1872-2067(18)63047-5
9. Lang R, Xi W, Liu JC et al (2019) Non defect-stabilized thermally stable single-atom catalyst. Nat Commun 10:1–10. https://doi.org/10.1038/s41467-018-08136-3
10. Zhang J, Wu X, Cheong WC et al (2018) Cation vacancy stabilization of single-atomic-site Pt 1 /Ni(OH) x catalyst for diboration of alkynes and alkenes. Nat Commun 9:1–8. https://doi.org/10.1038/s41467-018-03380-z
11. Wan J, Chen W, Jia C et al (2018) Defect effects on TiO_2 nanosheets: stabilizing single atomic site Au and promoting catalytic properties. Adv Mater 30(11):1705369. https://doi.org/10.1002/adma.201705369
12. Franchini C, Reticcioli M, Setvin M, Diebold U (2021) Polarons in materials. Nat Rev Mater 6:560–586. https://doi.org/10.1038/s41578-021-00289-w
13. Reticcioli M, Sokolović I, Schmid M et al (2019) Interplay between adsorbates and polarons: CO on rutile TiO_2 (110). Phys Rev Lett 122:1–6. https://doi.org/10.1103/PhysRevLett.122.016805
14. Sokolović I, Reticcioli M, Čalkovský M et al (2020) Resolving the adsorption of molecular O2 on the rutile TiO_2(110) surface by noncontact atomic force microscopy. Proc Natl Acad Sci USA 117:14827–14837. https://doi.org/10.1073/pnas.1922452117
15. Cao Y, Yu M, Qi S et al (2017) Scenarios of polaron-involved molecular adsorption on reduced TiO_2(110) surfaces. Sci Rep 7:1–7. https://doi.org/10.1038/s41598-017-06557-6
16. Papageorgiou AC, Beglitis NS, Pang CL et al (2010) Electron traps and their effect on the surface chemistry of TiO_2(110). Proc Natl Acad Sci USA 107:2391–2396. https://doi.org/10.1073/pnas.0911349107
17. Gono P, Wiktor J, Ambrosio F, Pasquarello A (2018) Surface polarons reducing overpotentials in the oxygen evolution reaction. ACS Catal 8:5847–5851. https://doi.org/10.1021/acscatal.8b01120
18. Lv CQ, Liu JH, Guo Y et al (2016) DFT + U investigation on the adsorption and initial decomposition of methylamine by a Pt single-atom catalyst supported on rutile (110) TiO_2. Appl Surf Sci 389:411–418. https://doi.org/10.1016/j.apsusc.2016.07.111
19. Wang J, Zhang W, Zhu W et al (2020) Rutile TiO2 supported single atom Au catalyst: a facile approach to enhance methanol dehydrogenation. Mol Catal 482:110670. https://doi.org/10.1016/j.mcat.2019.110670
20. Fung V, Hu G, Tao F, Jiang D (2019) Methane chemisorption on oxide-supported Pt single atom. ChemPhysChem 20:2217–2220. https://doi.org/10.1002/cphc.201900497
21. Ammal SC, Heyden A (2017) Titania-supported single-atom platinum catalyst for water-gas shift reaction. Chem-Ing-Tech 89:1343–1349. https://doi.org/10.1002/cite.201700046
22. Chang TY, Tanaka Y, Ishikawa R et al (2014) Direct imaging of pt single atoms adsorbed on TiO_2 (110) surfaces. Nano Lett 14:134–138. https://doi.org/10.1021/nl403520c
23. Tang Y, Asokan C, Xu M et al (2019) Rh single atoms on TiO_2 dynamically respond to reaction conditions by adapting their site. Nat Commun 10:1–10. https://doi.org/10.1038/s41467-019-12461-6
24. Reticcioli M, Setvin M, Schmid M et al (2018) Formation and dynamics of small polarons on the rutile TiO_2 (110) surface. Phys Rev B 98:45306. https://doi.org/10.1103/PhysRevB.98.045306
25. Setvin M, Franchini C, Hao X et al (2014) Direct view at excess electrons in TiO_2 rutile and anatase. Phys Rev Lett 113:1–5. https://doi.org/10.1103/PhysRevLett.113.086402

26. Janotti A, Franchini C, Varley JB et al (2013) Dual behavior of excess electrons in rutile TiO_2. Phys Status Solidi Rapid Res Lett 7:199–203. https://doi.org/10.1002/pssr.201206464
27. Nørskov JK, Bligaard T, Rossmeisl J, Christensen CH (2009) Towards the computational design of solid catalysts. Nat Chem 1:37–46. https://doi.org/10.1038/nchem.121
28. Corma A (2016) Heterogeneous catalysis: understanding for designing, and designing for applications. Angew Chem Int Ed 55:6112–6113. https://doi.org/10.1002/anie.201601231
29. Zhao ZJ, Chiu CC, Gong J (2015) Molecular understandings on the activation of light hydrocarbons over heterogeneous catalysts. Chem Sci 6:4403–4425. https://doi.org/10.1039/c5sc01227a
30. Li L, Chang X, Lin X et al (2020) Theoretical insights into single-atom catalysts. Chem Soc Rev 49:8156–8178. https://doi.org/10.1039/d0cs00795a
31. Chrétien S, Metiu H (2007) Density functional study of the interaction between small Au clusters, Aun (n = 1–7) and the rutile TiO_2 surface. II. Adsorption on a partially reduced surface. J Chem Phys 127:244708. https://doi.org/10.1063/1.2806802
32. Pillay D, Hwang GS (2005) Growth and structure of small gold particles on rutile TiO_2(110). Phys Rev B 72:1–6. https://doi.org/10.1103/PhysRevB.72.205422
33. Pillay D, Wang Y, Hwang GS (2004) A comparative theoretical study of Au, Ag and Cu adsorption on TiO_2 (110) rutile surfaces. Korean J Chem Eng 21:537–547. https://doi.org/10.1007/BF02705445
34. Okazaki K, Morikawa Y, Tanaka S et al (2004) Electronic structures of Au on TiO_2(110) by first-principles calculations. Phys Rev B 69:1–8. https://doi.org/10.1103/PhysRevB.69.235404
35. Mellor A, Humphrey D, Yim CM et al (2017) Direct visualization of au atoms bound to TiO_2(110) O-vacancies. J Phys Chem C 121:24721–24725. https://doi.org/10.1021/acs.jpcc.7b09608
36. Kresse G, Furthmüller J (1996) Efficiency of ab-initio total energy calculations for metals and semiconductors using a plane-wave basis set. Comput Mater Sci 6:15–50. https://doi.org/10.1016/0927-0256(96)00008-0
37. Vargas-Hernández RA (2020) Bayesian optimization for calibrating and selecting hybrid-density functional models. J Phys Chem A 124:4053–4061. https://doi.org/10.1021/acs.jpca.0c01375
38. Blöchl PE (1994) Projector augmented-wave method. Phys Rev B 50:17953–17979. https://doi.org/10.1103/PhysRevB.50.17953
39. Joubert D (1999) From ultrasoft pseudopotentials to the projector augmented-wave method. Phys Rev B 59:1758–1775. https://doi.org/10.1103/PhysRevB.59.1758
40. Dion M, Rydberg H, Schröder E et al (2004) Van der Waals density functional for general geometries. Phys Rev Lett 92:22–25. https://doi.org/10.1103/PhysRevLett.92.246401
41. Klimeš J, Bowler DR, Michaelides A (2010) Chemical accuracy for the van der Waals density functional. J Phys Condens Matter 2(22):022201. https://doi.org/10.1088/0953-8984/22/2/022201
42. Klime J, Bowler DR, Michaelides A (2011) Van der Waals density functionals applied to solids. Phys Rev B 83:1–13. https://doi.org/10.1103/PhysRevB.83.195131
43. Giustino F (2017) Electron-phonon interactions from first principles. Rev Mod Phys 89:1–63. https://doi.org/10.1103/RevModPhys.89.015003
44. Maxisch T, Zhou F, Ceder G (2006) Ab initio study of the migration of small polarons in olivine Lix FePO4 and their association with lithium ions and vacancies. Phys Rev B 73:1–6. https://doi.org/10.1103/PhysRevB.73.104301
45. Nolan M, Watson GW (2006) Hole localization in Al doped silica: A DFT + U description. J Chem Phys 125(14):144701. https://doi.org/10.1063/1.2354468
46. Wang Z, Brock C, Matt A, Bevan KH (2017) Implications of the DFT + U method on polaron properties in energy materials. Phys Rev B 96:1–13. https://doi.org/10.1103/PhysRevB.96.125150
47. Deskins NA, Rousseau R, Dupuis M (2011) Distribution of Ti3 + surface sites in reduced TiO_2. J Phys Chem C 115:7562–7572. https://doi.org/10.1021/jp2001139
48. Di Valentin C, Pacchioni G, Selloni A (2006) Electronic structure of defect states in hydroxylated and reduced rutile TiO_2(110) surfaces. Phys Rev Lett 97(16):166803. https://doi.org/10.1103/PhysRevLett.97.166803
49. Henkelman G, Uberuaga BP, Jónsson H (2000) Climbing image nudged elastic band method for finding saddle points and minimum energy paths. J Chem Phys 113:9901–9904. https://doi.org/10.1063/1.1329672
50. Henkelman G, Jónsson H (2000) Improved tangent estimate in the nudged elastic band method for finding minimum energy paths and saddle points. J Chem Phys 113:9978–9985. https://doi.org/10.1063/1.1323224
51. Fernández-Torre D, Yurtsever A, Onoda J et al (2015) Pt atoms adsorbed on TiO_2(110)-(1×1) studied with noncontact atomic force microscopy and first-principles simulations. Phys Rev B 91:1–8. https://doi.org/10.1103/PhysRevB.91.075401
52. Wang X, Zhang L, Bu Y, Sun W (2021) Interplay between invasive single atom Pt and native oxygen vacancy in rutile TiO_2(110) surface: a theoretical study. Nano Res 12:4–11. https://doi.org/10.1007/s12274-021-3542-5
53. Matthey D, Wang JG, Wendt S et al (2007) Enhanced bonding of gold nanoparticles on oxidized TiO_2(110). Science 315:1692–1696. https://doi.org/10.1126/science.1135752
54. Giordano L, Pacchioni G, Bredow T, Sanz JF (2001) Cu, Ag, and Au atoms adsorbed on TiO_2(1 1 0): cluster and periodic calculations. Surf Sci 471:21–31. https://doi.org/10.1016/S0039-6028(00)00879-7
55. Allen JP, Watson GW (2014) Occupation matrix control of d- and f-electron localisations using DFT + U. Phys Chem Chem Phys 16:21016–21031. https://doi.org/10.1039/c4cp01083c
56. Huber F, Giessibl FJ (2017) Low noise current preamplifier for qPlus sensor deflection signal detection in atomic force microscopy at room and low temperatures. Rev Sci Instrum 29(7):073702. https://doi.org/10.1063/1.4993737
57. Choi JIJ, Mayr-Schmölzer W, Mittendorfer F et al (2014) The growth of ultra-thin zirconia films on Pd3Zr(0 0 0 1). J Phys Condens Matter 26(22):225003. https://doi.org/10.1088/0953-8984/26/22/225003
58. Lun Pang C, Lindsay R, Thornton G (2008) Chemical reactions on rutile TiO_2(110). Chem Soc Rev 37:2328–2353. https://doi.org/10.1039/b719085a
59. Diebold U (2003) Structure and properties of TiO_2 surfaces: a brief review. Appl Phys A 76:681–687. https://doi.org/10.1007/s00339-002-2004-5
60. Diebold U (2003) The surface science of titanium dioxide. Surf Sci Rep 48:53–229
61. Deák P, Aradi B, Frauenheim T (2012) Quantitative theory of the oxygen vacancy and carrier self-trapping in bulk TiO_2. Phys Rev B 86:1–8. https://doi.org/10.1103/PhysRevB.86.195206
62. Moses PG, Janotti A, Franchini C et al (2016) Donor defects and small polarons on the TiO_2(110) surface. J Appl Phys 119(18):181503. https://doi.org/10.1063/1.4948239
63. Valentin C, Di, Pacchioni G, Selloni A (2009) Reduced and n-type doped TiO_2: nature of Ti 3 + species. J Phys Chem C 113:20543–20552
64. Diebold U, Lehman J, Mahmoud T et al (1998) Intrinsic defects on a TiO_2(110)(1×1) surface and their reaction with oxygen: a scanning tunneling microscopy study. Surf Sci 411:137–153. https://doi.org/10.1016/S0039-6028(98)00356-2
65. Brookes IM, Muryn CA, Thornton G (2001) Imaging water dissociation on TiO_2(110). Phys Rev Lett. 110(43):21840. https://doi.org/10.1103/PhysRevLett.87.266103

66. Schaub R, Thostrup P, Lopez N et al (2001) Oxygen vacancies as active sites for water dissociation on rutile TiO_2(110). Phys Rev Lett. 87(26):266104. https://doi.org/10.1103/PhysRevLett.87.266104
67. Wendt S, Schaub R, Matthiesen J et al (2005) Oxygen vacancies on TiO_2(1 1 0) and their interaction with H2O and O2: a combined high-resolution STM and DFT study. Surf Sci 598:226–245. https://doi.org/10.1016/j.susc.2005.08.041
68. Du Y, Deskins NA, Zhang Z et al (2009) Imaging consecutive steps of O 2 reaction with hydroxylated TiO_2(110): identification of HO 2 and terminal OH intermediates. J Phys Chem C 113:666–671. https://doi.org/10.1021/jp807030n
69. Li L, Li W, Zhu C, Mao LF (2021) A DFT + U study about agglomeration of Au atoms on reduced surface of rutile TiO_2 (110). Mater Chem Phys 271:124944. https://doi.org/10.1016/j.matchemphys.2021.124944
70. Hugenschmidt MB, Gamble L, Campbell CT (1994) The interaction of H2O with a TiO_2(110) surface. Surf Sci 302:329–340. https://doi.org/10.1016/0039-6028(94)90837-0
71. Mellor A, Wilson A, Pang CL et al (2020) Photoemission core level binding energies from multiple sized nanoparticles on the same support: TiO_2(110)/Au. J Chem Phys 152(2):024709. https://doi.org/10.1063/1.5135760
72. Williams OBJ, Katsiev K, Baek B et al (2022) Direct visualization of a gold nanoparticle electron trapping effect. J Am Chem Soc 144:1034–1044. https://doi.org/10.1021/jacs.1c12197
73. Chŕtien S, Metiu H (2007) Density functional study of the charge on Aun clusters (n = 1–7) supported on a partially reduced rutile TiO_2 (110): are all clusters negatively charged? J Chem Phys. https://doi.org/10.1063/1.2709886
74. Birschitzky VC, Ellinger F, Diebold U et al (2022) Machine learning for exploring small polaron configurational space. https://doi.org/10.48550/arXiv.2202.01042

Publisher's Note Springer Nature remains neutral with regard to jurisdictional claims in published maps and institutional affiliations.